ARTICLE Open Access

Distinct superconducting properties and hydrostatic pressure effects in 2D α- and β-Mo$_2$C crystal sheets

Yunjie Fan[1], Chuan Xu[2], Xiang Liu[1], Chao Ma[1], Yuewei Yin [1], Hui-Ming Cheng [2,3], Wencai Ren [2,3] and Xiaoguang Li [1,4,5]

Abstract

Recently, 2D Mo$_2$C, a new member of the MXene family, has attracted much attention due to the exotic superconducting properties discovered in 2D α-Mo$_2$C. Here, not only 2D α-Mo$_2$C but also 2D β-Mo$_2$C crystal sheets with distinct disordered carbon distributions were successfully grown. 2D β-Mo$_2$C shows a much stronger superconductivity than 2D α-Mo$_2$C, and their superconductivities have different hydrostatic pressure responses. The superconducting transition temperature T_c of 2D α-Mo$_2$C shows a dome-shaped profile under pressure, implying the existence of two competing effects arising from phononic and electronic properties, while for 2D β-Mo$_2$C, T_c decreases monotonically with increasing pressure, possibly due to phonon stiffening. These results indicate that the electronic properties have a more important influence on the superconductivity in 2D α-Mo$_2$C compared to 2D β-Mo$_2$C. The ordered and disordered carbon distributions in 2D α-Mo$_2$C and β-Mo$_2$C, respectively, may be the underlying origin for their different electronic and superconducting properties.

Introduction

In the past few years, MXenes, i.e., two-dimensional transition metal carbides (2D TMCs), have received increasing attention due to their tremendous potential for electromagnetic interference shielding, energy storage, catalysis, and electronic devices[1–5]. As one of the most widely studied 2D TMCs, ultrathin molybdenum carbide (Mo$_2$C) not only shows a high electronic conductivity but also exhibits exotic superconducting properties at low temperatures[6]. Orthorhombic α-Mo$_2$C and hexagonal β-Mo$_2$C are the two stable crystalline forms of the Mo$_2$C family, but they show distinct ordered and disordered carbon atom distributions, respectively, in almost identical Mo matrices[7,8]. Early reports showed that the superconducting transition temperatures (T_c) of α-Mo$_2$C and β-Mo$_2$C in bulk form lie within wide ranges of 4–12.2 K and 2.4–7.2 K, respectively, due to the inconsistent sample qualities and possible impurity phases[8].

Recently, Xu et al. successfully synthesized high-quality 2D α-Mo$_2$C crystal sheets with a chemical vapor deposition (CVD) process[6]. This triggered the discovery of many intriguing properties in this promising 2D TMC system, including 2D superconductivity[6], quantum phase transitions[7,9], nonlinear optical properties[10], and fantastic physics at the interfaces between α-Mo$_2$C and other 2D materials[2,11]. The T_c of α-Mo$_2$C crystal sheets is as high as 3.5 K and becomes lower in thinner crystal sheets, and the superconductivity is suppressed locally at grain boundaries[6,12,13]. Interestingly, disorder-enhanced superconductivity in α-Mo$_2$C sheets was observed very recently by scanning tunneling microscopy, which was attributed

Correspondence: Yuewei Yin (yyw@ustc.edu.cn) or Wencai Ren (wcren@imr.ac.cn) or Xiaoguang Li (lixg@ustc.edu.cn)
[1]Hefei National Laboratory for Physical Sciences at the Microscale, Department of Physics, and CAS Key Laboratory of Strongly-coupled Quantum Matter Physics, University of Science and Technology of China, Hefei 230026, China
[2]Shenyang National Laboratory for Materials Science, Institute of Metal Research, Chinese Academy of Sciences, Shenyang 110016, China
Full list of author information is available at the end of the article
These authors contributed equally: Yunjie Fan, Chuan Xu, Xiang Liu

to lattice defect-enhanced disordering and strain-induced strong coupling[14]. In addition to the interesting electronic properties, 2D Mo_2C also exhibits unique structural properties. Polarized Raman spectroscopy and transmission electron microscopy studies on 2D α-Mo_2C crystal sheets revealed unique domain structures with 60° and 120° boundaries[15]. In particular, it was found that the domain structures can be eliminated and the α-Mo_2C sheets can be transformed into β-Mo_2C by electron beam irradiation[7]. Considering the distinct ordered and disordered carbon atom distributions in α-Mo_2C and β-Mo_2C, respectively, this unique structural feature should have important impacts on the superconductivity owing to the close interaction between the electronic and structural characteristics. However, there are still no reports about the superconductivity in the 2D β-Mo_2C crystal sheet and its differences with 2D α-Mo_2C.

In addition, the superconductivity can be significantly modulated by a basic thermodynamic variable, the hydrostatic pressure (P). A higher dT_c/dP of a superconductor implies that a suitable chemical substitution or epitaxial strain design at ambient pressure may be utilized to achieve an enhanced T_c[16,17]. In particular, research on the superconducting properties under high pressures may help uncover the superconducting mechanism by revealing the impacts of different competing orders in superconducting materials[18]. For instance, in simple metal superconductors with s or p orbital electronic conduction, such as Al, In, Sn, and Pb, a ubiquitous reduction in T_c was observed due to stiffening of lattice vibration spectra under pressure, suggesting the importance of phononic properties for the superconductivity[19]. For some transition metals with d orbital electronic conduction, such as Tl and Re, the pressure-modulated Fermi surface topology is important for the nonmonotonic pressure dependence of T_c, reflecting the critical role and complexity of their electronic properties[20,21]. For unconventional superconductors, such as high-temperature cuprate superconductors, T_c often shows a dome-like pressure dependence due to the complex and strongly correlated electronic effects[22,23]. However, there is still no research devoted to the pressure effects on the superconductivities of α-Mo_2C and β-Mo_2C thus far. Pressure studies may shed light on the understanding of the superconductivities in Mo_2C of these two structures with different carbon atom distributions.

In this work, the crystal structures and superconductivities of 2D α-Mo_2C and β-Mo_2C sheets were systematically studied. By investigating the electronic transport and superconducting properties under hydrostatic pressures, it was discovered that their T_c, upper critical fields (H_{c2}), pressure responses of the superconductivity, and transport behaviors in normal states are quite different. These different electronic properties may

be highly related to the different carbon atom distributions in the α-Mo_2C and β-Mo_2C sheets.

Materials and methods
Sample preparation

CVD with a Cu/Mo bilayer substrate was used to grow 2D Mo_2C crystal sheets[6,13]. Different from our previous report[6], the formations of rectangular-shaped α-Mo_2C sheets and hexagonal-shaped β-Mo_2C sheets in the same batch were achieved by using a higher flow rate of methane of ~0.6 sccm[13]. The Mo_2C sheet crystals were transferred onto TEM grids for structural characterizations and 10 mm × 10 mm SiO_2 (300 nm)/Si substrates for transport measurements[6].
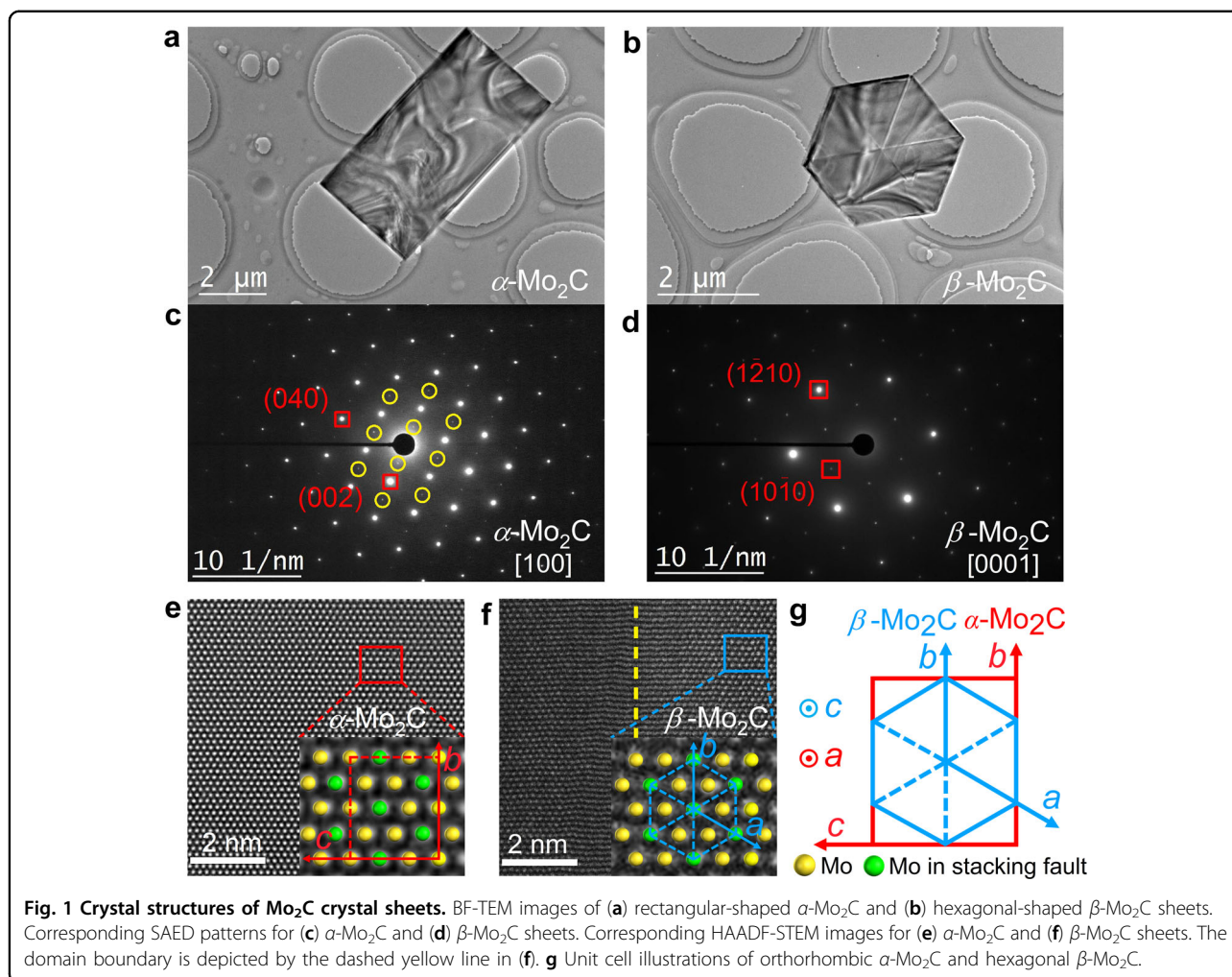
Characterizations

The structures were investigated by high angle angular dark field (HAADF)-scanning transmission electron microscopy (STEM) and corresponding selected area electron diffraction (SAED) by TEM with a spherical aberration corrector (Talos F200X). The sample thicknesses were measured by an atomic force microscope (Oxford MFP-3D Infinity). Electron-beam lithography (JEOL JBX-6300FS) and a lift-off process were used to prepare Ti/Au (10/90 nm) electrodes, and e-beam irradiation at 100 kV and 10 nA was performed in the electron-beam lithography equipment. A Quantum Design Physical Property Measurement System (QD PPMS 9 T) with an HPC-33 piston-type pressure cell (Daphne 7373 oil as the pressure transmitting medium) was used to perform the resistance measurements at different magnetic fields under various pressures. The superconducting transition temperature of Sn was used to calibrate the magnitude of the pressure.

Results and discussion
Structural characteristics of 2D α-Mo_2C and β-Mo_2C crystal sheets

As reported previously[6], 2D α-Mo_2C crystals grown by CVD at a low flow rate of methane mainly have 6 kinds of regular shapes (hexagons, rectangles, triangles, etc.), indicating a typical characteristic of good crystallization. In contrast, the 2D Mo_2C sheets used in our study were grown by CVD with a high flow rate of methane and were mostly rectangular and hexagonal, with lateral sizes of 10–20 μm and thicknesses (d) of 5–30 nm. The thicknesses of the sheets were measured by atomic force microscopy, and representative images are shown in Supplementary Fig. S1. The superconducting properties of Mo_2C crystal sheets are highly stable under ambient conditions due to their excellent thermal and chemical stabilities.

High-resolution STEM was utilized to characterize the crystal structures of the Mo_2C sheets. Figure 1a, b shows

Fig. 1 Crystal structures of Mo₂C crystal sheets. BF-TEM images of (**a**) rectangular-shaped α-Mo₂C and (**b**) hexagonal-shaped β-Mo₂C sheets. Corresponding SAED patterns for (**c**) α-Mo₂C and (**d**) β-Mo₂C sheets. Corresponding HAADF-STEM images for (**e**) α-Mo₂C and (**f**) β-Mo₂C sheets. The domain boundary is depicted by the dashed yellow line in (**f**). **g** Unit cell illustrations of orthorhombic α-Mo₂C and hexagonal β-Mo₂C.
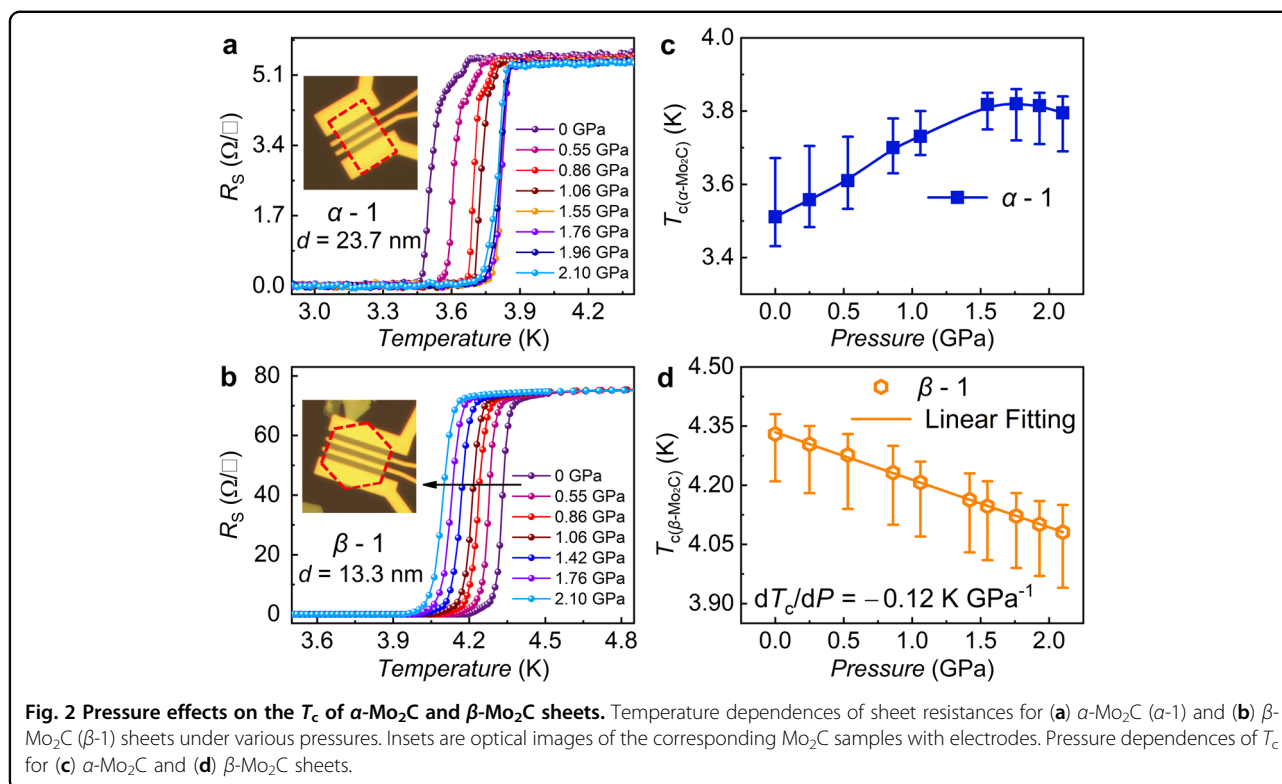
bright-field TEM images of the Mo_2C crystal sheets of rectangular and hexagonal shapes, respectively, and Fig. 1c, d shows the corresponding SAED patterns. It can be seen that the rectangular- and hexagonal-shaped Mo_2C sheets have different crystal lattice symmetries. The rectangular-shaped sheets of Mo_2C are of the α-phase with an orthorhombic structure. As for the hexagonal-shaped sheets, they are of the β-phase with a hexagonal structure. Moreover, the α-Mo_2C sheet grows along the [100] direction, while the β-Mo_2C sheet grows along the [0001] direction, perpendicular to their surfaces. As highlighted by the yellow circles in the SAED pattern shown in Fig. 1c, superlattice diffraction spots are observed for the α-Mo_2C sheets. This feature has been proven to result from the ordered distribution of carbon atoms, which attract each other in the Mo octahedrons, leading to a regular distortion of the hexagonal close-packed Mo lattice[7,8,24]. In contrast, there is no Mo lattice distortion in the β-Mo_2C sheets because the disordered distribution of carbon atoms mutually offsets the interactions[7]. It is worth mentioning that the α-Mo_2C sheets

can be transformed into β-Mo_2C by the electron beam irradiation-induced order-disorder transition[7]. In other words, β-Mo_2C is a disordered counterpart of the ordered α-Mo_2C phase at high temperature[25].

Figure 1e, f shows atomic-resolution HAADF-STEM images of α-Mo_2C and β-Mo_2C sheets, respectively. As seen from the magnified images shown in the insets of Fig. 1e, f, there exist extra Mo lattice points (denoted by the green spheres) located at the centers of Mo hexagons, which is due to the stacking faults in the growth direction[26]. In addition, it can be seen that the Mo atoms in the α-Mo_2C (along the [100] zone axis) and β-Mo_2C (along the [0001] zone axis) sheets have very similar atomic configurations. Actually, α-Mo_2C and β-Mo_2C are closely crystallographically related, namely, $a_\alpha = c_\beta$, $b_\alpha = 2b_\beta$, and $c_\alpha = \sqrt{3}a_\beta$, as illustrated in Fig. 1g. Therefore, considering the almost identical Mo lattices, the main structural difference between α-Mo_2C and β-Mo_2C sheets is the different distributions of carbon atoms.

Another interesting feature is the presence of diagonal domain boundaries in hexagonal β-Mo_2C sheets, as

Fig. 2 Pressure effects on the T_c of α-Mo$_2$C and β-Mo$_2$C sheets. Temperature dependences of sheet resistances for (**a**) α-Mo$_2$C (α-1) and (**b**) β-Mo$_2$C (β-1) sheets under various pressures. Insets are optical images of the corresponding Mo$_2$C samples with electrodes. Pressure dependences of T_c for (**c**) α-Mo$_2$C and (**d**) β-Mo$_2$C sheets.

shown in Fig. 1b. An atomic-resolution HAADF-STEM image near the boundary is shown in Fig. 1f, and the domain boundary is highlighted by the yellow dashed line. Interestingly, the lattice remains unchanged on the two sides of the boundary. The SAED patterns in each domain area are also studied (Supplementary Fig. S2), and the same SAED patterns in all areas indicate that the crystal structure is uniform throughout the whole crystal. It should be noted that diagonal domain boundaries have also been observed in hexagonal-shaped orthorhombic α-Mo$_2$C crystal sheets, but the lattice of the adjacent domain areas rotates by 60° in plane, which results in different SAED patterns in the neighboring domains[15,24]. Moreover, the fringe contrast at the domain boundary in Fig. 1f indicates that there exists a translational strain of the Mo lattice at the domain boundary of β-Mo$_2$C sheets, which is also different from the feature of α-Mo$_2$C sheets[15,24].

Hydrostatic pressure responses of the superconductivities in 2D α-Mo$_2$C and β-Mo$_2$C crystal sheets

With the distinct structural features, it will be interesting to study the transport property differences between the α-Mo$_2$C and β-Mo$_2$C sheets by tuning a thermodynamic variable—pressure. Figure 2a, b shows the temperature dependences of the sheet resistances (R_s) for a 23.7-nm-thick α-Mo$_2$C sheet (labeled α-1) and a 13.3-nm-

thick β-Mo$_2$C sheet (labeled β-1) at various hydrostatic pressures. R_s is defined by $R_s = \rho/d = RW/L$, where W is the width and L is the length. Obviously different pressure effects on T_c were observed for α-Mo$_2$C and β-Mo$_2$C sheets, as the pressure dependences of T_c in Fig. 2c, d show. Here, the top and bottom lines of the error bars are the onset temperature $T_{c,onset}$ and zero resistance temperature $T_{c,zero}$, respectively, and $T_{c,onset}$, T_c, and $T_{c,zero}$ are defined by the resistance dropping to 90%, 50%, and 0.1% of the normal state resistance, respectively[27,28]. For α-Mo$_2$C sheets, T_c first increases and then decreases with increasing pressure, presenting a dome-like shape. For β-Mo$_2$C sheets with T_c higher than that of α-Mo$_2$C sheets, a monotonic reduction in T_c under pressure with $dT_c/dP = -0.12$ K GPa^{-1} was obtained for β-1. Similar measurements were also performed for a 25.1-nm-thick α-Mo$_2$C sample (labeled α-2) and a 7.1-nm-thick β-Mo$_2$C sample (labeled β-2, $dT_c/dP = -0.10$ K GPa^{-1}), and consistent pressure effects were observed (Supplementary Fig. S3). In addition, we noted that the resistivity transitions in some of the samples, such as α-1 (Fig. 2a) and β-2 (Fig. S3b), show pronounced shoulders, which may be due to sample inhomogeneity[29] (such as domain boundaries[24]) and/or electrode contact quality.

Here, the hydrostatic pressure effect on the superconductivity of Mo$_2$C can be discussed in the BCS framework[30,31]. Typically, the hydrostatic pressure

dependences of T_c for BCS superconductors can be analyzed in terms of McMillan theory as follows[32]:

$$T_{\mathrm{c}} = \frac{\Theta_D}{1.45}\exp\left\{\frac{-1.04(1+\lambda)}{\lambda - \mu^*(1+0.62\lambda)}\right\}. \quad (1)$$

Here, Θ_D is the Debye temperature, λ is the electron-phonon coupling parameter, and the Coulomb pseudo-potential μ^* is equal to 0.1 and is insensitive to pressure[21,33,34]. Equation (1) has successfully described the pressure-manipulated T_c in many systems, including elemental superconductors[19], transition-metal nitrides[35], MgB_2[36], LaH_{10}[37], etc[34]. Based on Eq. (1), the following relationship can be obtained by the logarithmic volume derivative[33]:

$$\frac{\mathrm{d}\ln T_{\mathrm{c}}}{\mathrm{d}\ln V} = -B\frac{\mathrm{d}\ln T_{\mathrm{c}}}{\mathrm{d}P} = -\gamma + \Delta\left\{\frac{\mathrm{d}\ln\eta}{\mathrm{d}\ln V}+2\gamma\right\}, \quad (2)$$

where V is the sample volume and B is the bulk modulus parameter. $\eta = N(E_{\mathrm{F}})\langle I^2\rangle$ is the product of the Fermi-level density of states $N(E_{\mathrm{F}})$ with the average squared electronic matrix element $\langle I^2\rangle$. $\gamma = -\mathrm{d}\ln\langle\omega\rangle/\mathrm{d}\ln V$ is the Grüneisen parameter, $\langle\omega\rangle$ is the mean phonon frequency, and $\Delta = 1.04\lambda[1+0.38\mu^*][\lambda - \mu^*(1+0.62\lambda)]^{-2}$ [38]. It can be seen that Eq. (2) contains the electron-phonon coupling, the density of states at the Fermi level, and the energy scale of the phonon excitations (Debye frequency). The terms $\gamma = -\mathrm{d}\ln\langle\omega\rangle/\mathrm{d}\ln V$ and $\mathrm{d}\ln\eta/\mathrm{d}\ln V$ represent the variations in the lattice and electronic characteristics with volume, respectively. It has been noted that the electronic term $\mathrm{d}\ln\eta/\mathrm{d}\ln V$ typically equals -1 for simple metal superconductors (s, p orbital electrons)[39] and -3 to -4 for transition metal superconductors (d orbital electrons)[21,33]. For Mo_2C, $N(E_{\mathrm{F}})$ is mainly contributed by the $4d$ orbitals of the molybdenum atoms[40]. According to Eq. (2), the negative electronic term $\mathrm{d}\ln\eta/\mathrm{d}\ln V$ tends to enhance T_c under pressure[21]. However, for most BCS superconductors, the effect from the pressure-induced phonon stiffening (i.e., $\gamma > 0$) overcomes the effect related to the change in electronic properties, which leads to a ubiquitous decrease in T_c[21].

For β-Mo_2C sheets, the negative $\mathrm{d}T_c/\mathrm{d}P = -0.12$ K GPa^{-1} means a positive $-B\mathrm{d}\ln T_c/\mathrm{d}P$ on the left side of Eq. (2). Using $T_c = 4.33$ K at ambient pressure, $\Theta_D = 590$ K[41], and $\mu^* = 0.1$, we obtained $\lambda = 0.46$ and $\Delta = 4.46$ from Eq. (1). The electron–phonon coupling parameter $\lambda = 0.46$ is in agreement with the value $\lambda = 0.5$ obtained from first-principles density-functional theory calculations[30]. Inserting these values, $\mathrm{d}T_c/\mathrm{d}P = -0.12$ K GPa^{-1}, $\mathrm{d}\ln\eta/\mathrm{d}\ln V = -3$ to -4, and $B \sim 290$ GPa[41], into Eq. (2), we obtain $\gamma = 2.7$ to 3.3. The large and positive γ suggests significant stiffening of the lattice vibration spectrum under pressure, which results in the reduction in T_c in β-Mo_2C sheets.

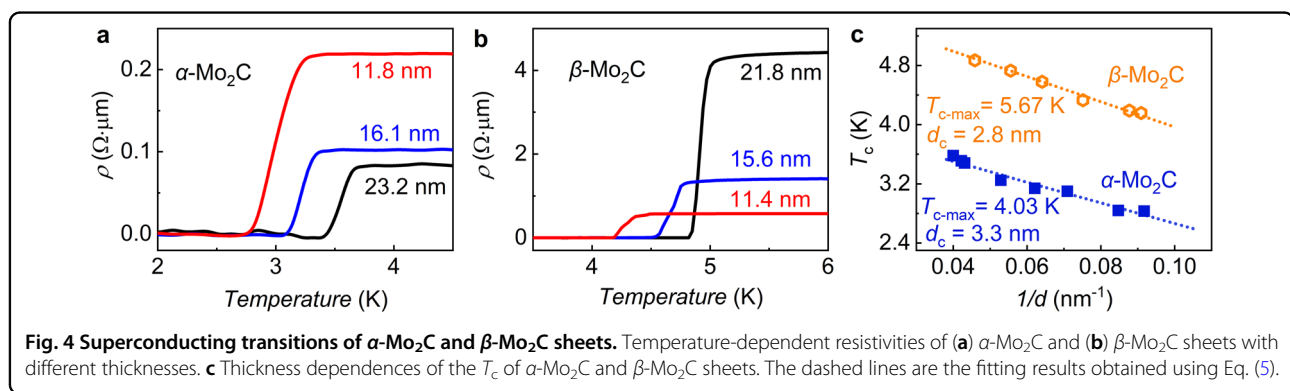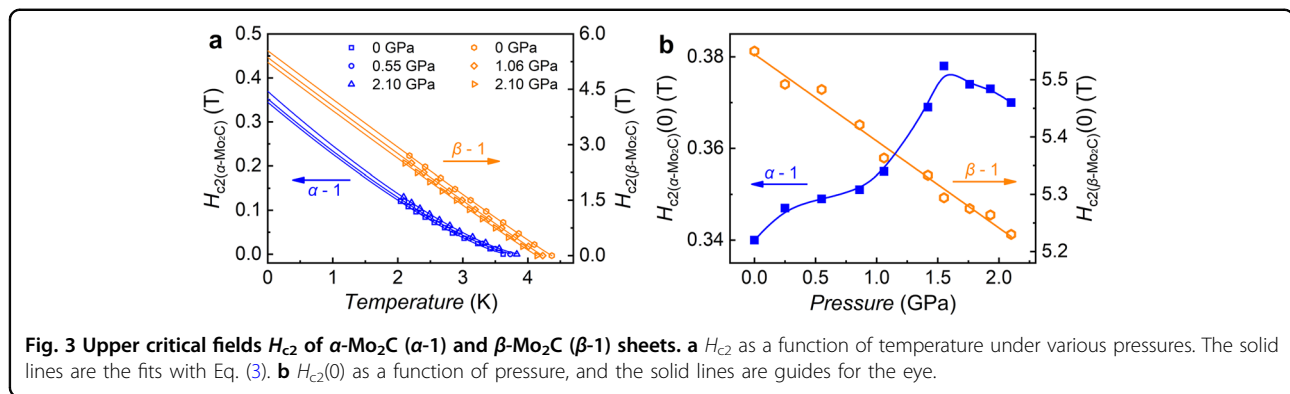For α-Mo_2C sheets, T_c first increases under low pressures and then decreases with further increases in pressure, leading to a distinct dome-like pressure dependence of T_c, which is obviously different from the decrease in T_c in β-Mo_2C sheets. Typically, an increase in T_c with pressure for a BCS superconductor occurs when the effect of the variation arising from the electronic characteristics with pressure overcomes the pressure-induced phonon stiffening effect. For example, in some BCS superconductors (e.g., Lu, Nb_3Ge, and $NbSe_2$), owing to the pressure-induced complex variation in electronic properties, T_c initially increases under low pressures[21,42,43]. Similarly, for α-Mo_2C sheets, the increase in T_c under low pressures may also be because the complex variation in electronic properties overcomes the phonon stiffening. For the decrease in T_c under high pressures, the phonon stiffening effect may overcome the electronic effect, similar to that in β-Mo_2C sheets. In other words, the distinct pressure responses of the superconductivities in α- and β-Mo_2C suggest their different electronic and phononic properties under pressure. Compared with the always dominant lattice effect in β-Mo_2C sheets, both the lattice and electronic effects play an important role in α-Mo_2C sheets, which may be related to their different carbon atom distributions. The more significant influence of the electronic term in α-Mo_2C should be related to the ordered carbon atoms, while the strong phonon stiffening effect in β-Mo_2C with randomly distributed carbon atoms may be due to the less sensitive pressure response of its electronic characteristic.

Upper critical fields H_{c2} of 2D α-Mo_2C and β-Mo_2C crystal sheets

To further understand the different superconducting characteristics of α-Mo_2C and β-Mo_2C sheets, their upper critical fields $H_{c2}(T)$ (defined by the resistance dropping to 90% of the normal state resistance[28]) were studied under various pressures. Based on the temperature-dependent resistances measured in various perpendicular magnetic fields under different pressures (Supplementary Fig. S4), the upper critical fields $H_{c2}(T)$ of α-Mo_2C (sample α-1) and β-Mo_2C (sample β-1) sheets are shown in Fig. 3a. For 2D superconducting systems, $H_{c2}(T)$ can be well fitted by the following relationship[44,45]:

$$H_{c2}(T) = H_{c2}(0)\left(1 - T/T_{c,\mathrm{onset}}\right)^{1+\alpha}, \quad (3)$$

where $H_{c2}(0)$ and α are the fitting parameters, and $\alpha \sim 0.34$ and $\alpha \sim 0.04$ are obtained for α-1 and β-1, respectively. Figure 3b shows the pressure dependences of $H_{c2}(0)$ for α-1 and β-1 sheets with distinct nonmonotonic and monotonic curvatures, respectively. At ambient pressure, the $H_{c2}(0)$ for α-Mo_2C sheets is 0.34 T, comparable with earlier reports[6,13], while the $H_{c2}(0)$ of 5.55 T for β-Mo_2C

Fig. 3 Upper critical fields H_{c2} of α-Mo$_2$C (α-1) and β-Mo$_2$C (β-1) sheets. a H_{c2} as a function of temperature under various pressures. The solid lines are the fits with Eq. (3). **b** $H_{c2}(0)$ as a function of pressure, and the solid lines are guides for the eye.

Fig. 4 Superconducting transitions of α-Mo$_2$C and β-Mo$_2$C sheets. Temperature-dependent resistivities of (**a**) α-Mo$_2$C and (**b**) β-Mo$_2$C sheets with different thicknesses. **c** Thickness dependences of the T_c of α-Mo$_2$C and β-Mo$_2$C sheets. The dashed lines are the fitting results obtained using Eq. (5).

sheets is ~16 times that for α-Mo$_2$C sheets. The initial slopes $dH_{c2}/dT|_{T=T_{c,onset}}$ for the α-Mo$_2$C and β-Mo$_2$C sheets are −0.06 and −1.11, respectively, and they are almost independent of pressure. Moreover, similar measurements were also performed for the $H_{c2}(T)$ in α-Mo$_2$C (sample α-3, $d = 18.9$ nm) and β-Mo$_2$C (sample β-3, $d = 15.6$ nm) sheets in parallel magnetic fields, and much larger $H_{c2}(0)$ in parallel magnetic fields than that in perpendicular magnetic fields can be observed, as expected for 2D superconductor systems (Supplementary Fig. S6).

The α-Mo$_2$C sheet with an ordered carbon atom distribution was considered to be a clean superconductor[6], while for β-Mo$_2$C, it should be treated as a dirty superconductor system due to its disordered carbon atom distribution. Typically, for a dirty superconductor, H_{c2} is highly related to the mean free path l and the coherence length $ξ$ as follows[46]:
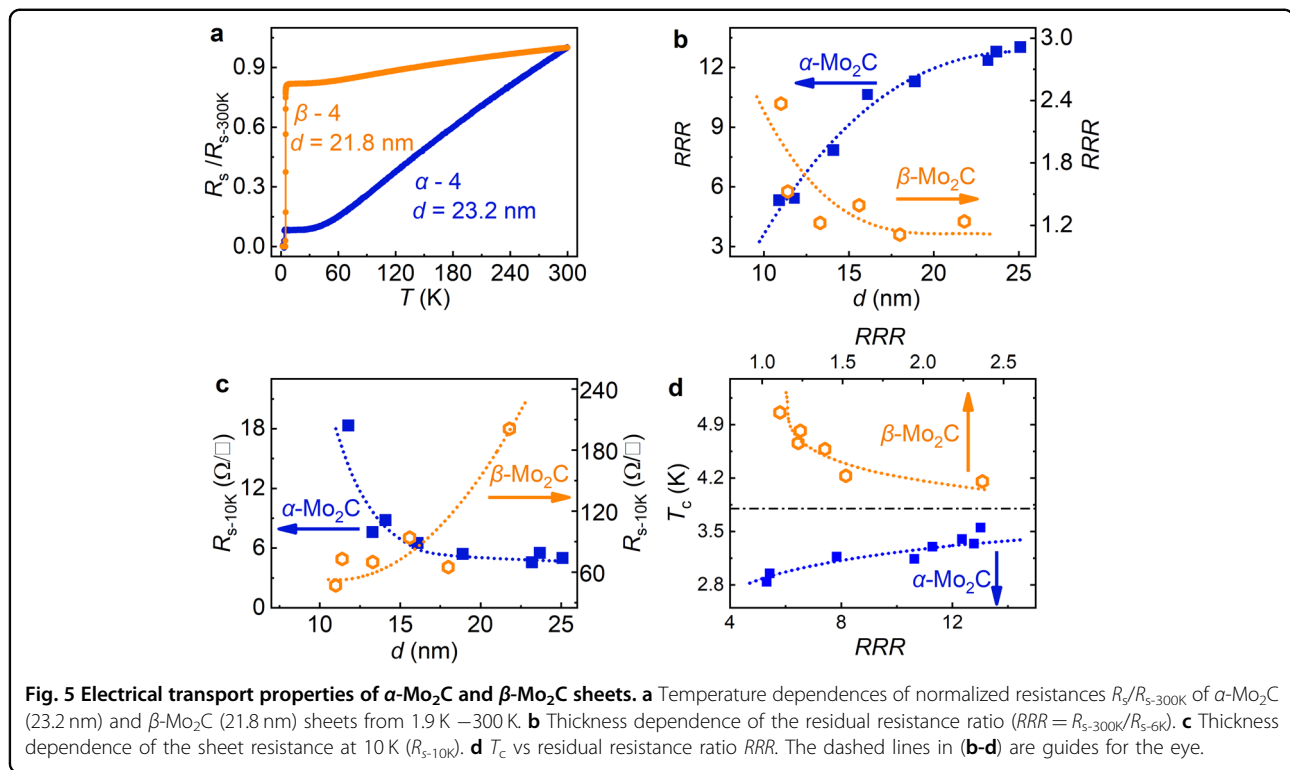
$$H_{c2}(0) \approx \Phi_0/2\pi\xi l \propto 3\times 10^4 T_c/v_F l, \qquad (4)$$

where Φ_0 is the magnetic flux quantum and v_F is the Fermi velocity. The product $v_F l$ is proportional to the electron diffusion coefficient, and a smaller $v_F l$ typically indicates stronger disorder[47,48]. According to Eq. (4), the H_{c2} of β-Mo$_2$C should be proportional to its T_c and inversely proportional to $v_F l$. Therefore, the dramatic

enhancement of the H_{c2} in β-Mo$_2$C can be due to its higher T_c and smaller $v_F l$ induced by the disordered carbon atom distribution. From the above discussions, it can be seen that the significant differences between α-Mo$_2$C and β-Mo$_2$C sheets should be related to the electronic structure differences, which are affected by the ordered and disordered carbon distributions. The detailed contributions of the ordered and disordered carbon atom distributions to the electronic structures of Mo$_2$C require further theoretical studies in the future.

Relationships among the thickness, residual resistivity ratio, and superconductivity of samples

For 2D sheets, the sample thickness generally has a significant influence on the electronic transport properties[49,50]. It is thus interesting to study the effects of thickness on the superconductivities of α-Mo$_2$C and β-Mo$_2$C sheets. Figure 4a, b shows the superconducting transitions of representative α-Mo$_2$C and β-Mo$_2$C crystal sheets with different sheet thicknesses, respectively. It can be seen that the values of T_c decrease with decreasing thickness for both α-Mo$_2$C and β-Mo$_2$C crystal sheets. Typically, in many superconducting systems, T_c is maximum ($T_{c\text{-max}}$) in the bulk sample and gradually decreases with decreasing sample thickness, and when the thickness is below a certain level (d_c), the sample will no longer be in the superconducting state[51,52]. Based on the Ginzburg-

Fig. 5 Electrical transport properties of α-Mo$_2$C and β-Mo$_2$C sheets. a Temperature dependences of normalized resistances $R_s/R_{s\text{-}300K}$ of α-Mo$_2$C (23.2 nm) and β-Mo$_2$C (21.8 nm) sheets from 1.9 K −300 K. **b** Thickness dependence of the residual resistance ratio ($RRR = R_{s\text{-}300K}/R_{s\text{-}6K}$). **c** Thickness dependence of the sheet resistance at 10 K ($R_{s\text{-}10K}$). **d** T_c vs residual resistance ratio RRR. The dashed lines in (**b-d**) are guides for the eye.

Landau equations, Simonin proposed a relationship between T_c and the thickness as follows[53,54]:

$$T_c = T_{c\text{-}max}(1 - d_c/d). \tag{5}$$

Figure 4c shows the evolution of T_c as a function of the inverse of the thickness ($1/d$), and the experimental results can be fitted very well by Eq. (5) with $T_{c\text{-}max} = 4.03$ K and $d_c = 3.3$ nm (~ 7 unit cells) for α-Mo$_2$C sheets and $T_{c\text{-}max} = 5.67$ K and $d_c = 2.8$ nm (~ 6 unit cells) for β-Mo$_2$C sheets. The $T_{c\text{-}max}$ values of α- and β-Mo$_2$C fall in the ranges of their bulk T_c of 4 K-12.2 K and 2.4 K-7.2 K[8], respectively, and the Mo$_2$C sheets may no longer be in a superconducting state when the sample thicknesses are below 6~7 unit cells[53]. Furthermore, the T_c of β-Mo$_2$C sheets is ~1.6 K higher than that of α-Mo$_2$C sheets with similar thicknesses. The higher T_c of β-Mo$_2$C than that of α-Mo$_2$C may be due to the enhanced electron-phonon coupling related to the disordered carbon distribution in β-Mo$_2$C[14] as well as the higher Debye temperature of β-Mo$_2$C (~590 K) than that of α-Mo$_2$C (~580 K)[41]. To further illustrate the role of the carbon distribution in Mo$_2$C, e-beam irradiation was used to produce varying degrees of disorder in the carbon distribution[7], and the order-disorder transition from α-Mo$_2$C to β-Mo$_2$C results in increases in T_c and the sheet resistance (Supplementary Figs. S7 and S8), consistent with Fig. 4.

According to the BCS superconducting mechanism, a stronger electron–phonon coupling, related to the intrinsic phononic and electronic properties, will lead to a higher T_c, which can be reflected by the normal state properties. For example, in elemental superconductors, a relatively strong electron-phonon coupling often results in a relatively poor electronic conduction[21,46], and disorder-enhanced electron-phonon coupling accompanied by an increase in resistivity was also observed in other superconductors, such as Mo$_3$Ge[55]. Thus, it will be interesting to study the normal state transport behaviors of α-Mo$_2$C and β-Mo$_2$C sheets. Figure 5a shows the temperature dependence of the normalized resistance $R_s/R_{s\text{-}300K}$ from 1.9 K to 300 K for representative α-Mo$_2$C (α-4, $d = 23.2$ nm) and β-Mo$_2$C (β-4, $d = 21.8$ nm) sheets with similar thicknesses. A faster decrease in the normal-state resistance with decreasing temperature was observed in the α-Mo$_2$C sheets, which indicates a stronger metallicity in the α-Mo$_2$C.

To obtain a more comprehensive assessment of the normal state properties of α-Mo$_2$C and β-Mo$_2$C sheets, the thickness dependences of their residual resistance ratio ($RRR = R_{s\text{-}300K}/R_{s\text{-}6K}$) and sheet resistance at 10 K ($R_{s\text{-}10K}$) are shown in Fig. 5b, c, respectively. Compared with α-Mo$_2$C sheets, β-Mo$_2$C shows a much smaller RRR and a much higher $R_{s\text{-}10K}$. In particular, the thickness-dependent trends for RRR and $R_{s\text{-}10K}$ are obviously

different between α-Mo$_2$C and β-Mo$_2$C sheets. A thicker α-Mo$_2$C sheet possesses a higher *RRR* and a smaller $R_{s\text{-}10K}$, while a thicker β-Mo$_2$C sheet has a lower *RRR* and a larger $R_{s\text{-}10K}$. A larger *RRR* means less electronic scattering, which will lead to a better electrical conductivity, namely, a smaller sheet resistance[56]. The electronic scattering in 2D sheet or film materials mainly results from two aspects: surface and/or interface scattering and intrinsic lattice scattering. In α-Mo$_2$C sheets, the intrinsic lattice scattering is relatively weak due to the ordered carbon atom distributions, and the surface scattering is dominant. Thus, for α-Mo$_2$C sheets, the importance of the surface scattering declines for thicker samples, which leads to an overall lower electronic scattering, a higher *RRR*, and a smaller sheet resistance. For β-Mo$_2$C sheets, the disordered carbon atom distributions will result in strong intrinsic lattice scattering. As a result, the overall stronger lattice scattering in a thicker β-Mo$_2$C sheet will lead to a smaller *RRR* and a larger sheet resistance.

Furthermore, the relationships between the T_c and *RRR* of α-Mo$_2$C and β-Mo$_2$C sheets plotted in Fig. 5d show different variation trends, and β-Mo$_2$C has a higher T_c with a smaller *RRR*, in contrast to α-Mo$_2$C. It is worth mentioning that a higher T_c usually accompanies a higher *RRR* due to the less scattering and higher sample quality[49,56], which is the case for α-Mo$_2$C sheets. In contrast, a higher T_c with a lower *RRR* was observed in the β-Mo$_2$C sheets. Considering the almost identical Mo lattices in α-Mo$_2$C and β-Mo$_2$C, it can be concluded that although the disordered distribution of carbon atoms increases the electronic scattering, it may promote the electron-phonon coupling and is beneficial for higher T_c, similar to Mo$_3$Ge[55].

Conclusions

In summary, the α- and β-phases of Mo$_2$C sheet crystals with rectangular and hexagonal shapes, respectively, were successfully grown by the CVD technique. It was found that the intriguing superconductivities in Mo$_2$C sheets of α- and β-phases have different hydrostatic pressure responses. Similar to conventional superconductors, β-Mo$_2$C sheets have a monotonic decrease in T_c under pressure due to the increase in the average vibration frequency of phonons, while the T_c of α-Mo$_2$C sheets shows a dome-shaped profile under pressure, which suggests the more critical role of the electronic properties in α-Mo$_2$C sheets. The β-Mo$_2$C sheets not only possess a higher T_c but also have a much larger H_{c2} (an order of magnitude larger than that of the α-Mo$_2$C sheets), which may be related to a stronger electron-phonon coupling strength as well as a smaller $v_F l$. Furthermore, the thickness-dependent T_c, *RRR*, and normal-state resistances were analyzed for α-Mo$_2$C and β-Mo$_2$C sheets, and the distinct thickness-dependent trends in the normal

state can be explained by the stronger lattice scattering in β-Mo$_2$C sheets. The distinct superconducting and normal-state electronic properties in α-Mo$_2$C and β-Mo$_2$C sheets should be related to their ordered and disordered carbon atom distributions, respectively. Our study provides a deep understanding of the superconductivity in α-Mo$_2$C sheets and lays the groundwork for future research into β-Mo$_2$C sheets, and the results may have great implications in the study of MXenes and superconductivity.

Author details
^{1}Hefei National Laboratory for Physical Sciences at the Microscale, Department of Physics, and CAS Key Laboratory of Strongly-coupled Quantum Matter Physics, University of Science and Technology of China, Hefei 230026, China. ^{2}Shenyang National Laboratory for Materials Science, Institute of Metal Research, Chinese Academy of Sciences, Shenyang 110016, China. ^{3}School of Material Science and Engineering, University of Science and Technology of China, Shenyang 110016, China. ^{4}Key Laboratory of Materials Physics, Institute of Solid State Physics, CAS, Hefei 230026, China. ^{5}Collaborative Innovation Center of Advanced Microstructures, Nanjing 210093, China

Author contributions
C.X. prepared the samples in the lab led by W.C.R. and H.M.C. X.L., Y.J.F., and C.M. performed the measurements. X.G.L., Y.W.Y., and W.C.R. designed and supervised the experiments. Y.J.F., X.L., W.C.R., Y.W.Y., and X.G.L. wrote the manuscript. All the authors contributed to the refinement of the manuscript. Y.J.F., C.X., and X.L. contributed equally.

Conflict of interest
The authors declare that they have no conflict of interest.

Publisher's note
Springer Nature remains neutral with regard to jurisdictional claims in published maps and institutional affiliations.

References
1. Anasori, B., Lukatskaya, M. R. & Gogotsi, Y. 2D metal carbides and nitrides (MXenes) for energy storage. *Nat. Rev. Mater.* **2**, 16098 (2017).
2. Hantanasirisakul, K. & Gogotsi, Y. Electronic and optical properties of 2D transition metal carbides and nitrides (MXenes). *Adv. Mater.* **30**, 1804779 (2018).
3. Shahzad, F. et al. Electromagnetic interference shielding with 2D transition metal carbides (MXenes). *Science* **353**, 1137–1140 (2016).
4. Ghidiu, M., Lukatskaya, M. R., Zhao, M.-Q, Gogotsi, Y. & Barsoum, M. W. Conductive two-dimensional titanium carbide 'clay' with high volumetric capacitance. *Nature* **516**, 78–82 (2014).

5. Lukatskaya, M. R. et al. Cation intercalation and high volumetric capacitance of two-dimensional titanium carbide. *Science* **341**, 1502–1505 (2013).

6. Xu, C. et al. Large-area high-quality 2D ultrathin Mo$_2$C superconducting crystals. *Nat. Mater.* **14**, 1135–1141 (2015).

7. Liu, Z. et al. Phase transition and in situ construction of lateral heterostructure of 2D superconducting alpha/beta Mo$_2$C with sharp interface by electron beam irradiation. *Nanoscale* **9**, 7501–7507 (2017).

8. Morton, N. et al. Superconductivity of molybdenum and tungsten carbides. *J. Less-Common Met.* **25**, 97–106 (1971).

9. Wang, L. et al. Magnetotransport properties in high-quality ultrathin two-dimensional superconducting Mo$_2$C crystals. *ACS nano* **10**, 4504–4510 (2016).

10. Tuo, M. F. et al. Ultrathin 2D transition metal carbides for ultrafast pulsed fiber lasers. *ACS Photonics* **5**, 1808–1816 (2018).

11. Xu, C. et al. Strongly coupled high-quality graphene/2D Superconducting Mo$_2$C vertical heterostructures with aligned orientation. *ACS Nano* **11**, 5906–5914 (2017).

12. Liu, Z. et al. Grain boundaries and tilt-angle-dependent transport properties of a 2D Mo$_2$C superconductor. *Nano Lett.* **19**, 857–865 (2019).

13. Geng, D. C. et al. Controlled growth of ultrathin Mo$_2$C superconducting crystals on liquid Cu surface. *2D Mater.* **4**, 011012 (2016).

14. Zhang, Z. et al. Layer-stacking, defects, and robust superconductivity on the Mo-terminated surface of ultrathin Mo$_2$C flakes grown by CVD. *Nano Lett.* **19**, 3327–3335 (2019).

15. Li, T., Luo, W., Kitadai, H., Wang, X. & Ling, X. Probing the domain architecture in 2D alpha-Mo$_2$C via polarized raman spectroscopy. *Adv. Mater.* **31**, 1807160 (2019).

16. Locquet, J.-P. et al. Doubling the critical temperature of La$_{1.9}$Sr$_{0.1}$CuO$_4$ using epitaxial strain. *Nature* **394**, 453–456 (1998).

17. Chen, X. H. et al. Superconductivity at 43 K in SmFeAsO$_{1-x}$F$_x$. *Nature* **453**, 761–762 (2008).

18. Sun, J. P. et al. Dome-shaped magnetic order competing with high-temperature superconductivity at high pressures in FeSe. *Nat. Commun.* **7**, 12146 (2016).

19. Olsen, J. L., Andres, K. & Geballe, T. H. The pressure dependence of the superconducting transition temperature. *Phys. Lett. A* **26**, 239–240 (1968).

20. Chu, C. W., Smith, T. F. & Gardner, W. E. Superconductivity of Rhenium and Some Rhenium-Osmium Alloys at High Pressure. *Phys. Rev. Lett.* **20**, 198–201 (1968).

21. Schrieffer, J. R. & Brooks, J. S. Handbook of high-temperature superconductivity theory and experiment. 427–462 (Springer-Verlag, 2007).

22. Sun, J. P. et al. High-T_c superconductivity in FeSe at high pressure: dominant hole carriers and enhanced spin fluctuations. *Phys. Rev. Lett.* **118**, 147004 (2017).

23. Sun, J. P. et al. Reemergence of high-T_c superconductivity in the (Li$_{1-x}$Fe$_x$)OHFe$_{1-y}$Se under high pressure. *Nat. Commun.* **9**, 380 (2018).

24. Liu, Z. et al. Unique domain structure of two-dimensional alpha-Mo$_2$C superconducting crystals. *Nano Lett.* **16**, 4243–4250 (2016).

25. Lönnberg, B. Thermal expansion studies on the subcarbides of group V and VI transition metals. *J. Less-Common Met.* **120**, 135–146 (1986).

26. Zhao, X. X. et al. Edge segregated polymorphism in 2D molybdenum carbide. *Adv. Mater.* **31**, 1808343 (2019).

27. Lin, X., Zhu, Z. W., Fauqué, B. & Behnia, K. Fermi surface of the most dilute superconductor. *Phys. Rev. X* **3**, 021002 (2013).

28. Fan, Y. J. et al. Quantum superconductor-insulator transition in titanium monoxide thin films with a wide range of oxygen contents. *Phys. Rev. B* **98**, 064501 (2018).

29. Gajar, B. et al. Substrate mediated nitridation of niobium into superconducting Nb$_2$N thin films for phase slip study. *Sci. Rep.* **9**, 8811 (2019).

30. Lei, J. C., Kutana, A. & Yakobson, B. I. Predicting stable phase monolayer Mo$_2$C (MXene), a superconductor with chemically-tunable critical temperature. *J. Mater. Chem. C.* **5**, 3438–3444 (2017).

31. Qiao, J.-B. et al. One-step synthesis of van der Waals heterostructures of graphene and two-dimensional superconducting α-Mo$_2$C. *Phys. Rev. B* **95**, 201403 (2017).

32. McMillan, W. L. Transition temperature of strong-coupled superconductors. *Phys. Rev.* **167**, 331–344 (1968).

33. Tomita, T., Hamlin, J. J., Schilling, J. S., Hinks, D. G. & Jorgensen, J. D. Dependence of T_c on hydrostatic pressure in superconducting MgB$_2$. *Phys. Rev. B* **64**, 092505 (2001).

34. Okaz, A. M. & Keesom, P. H. Specific heat and magnetization of the superconducting monoxides: NbO and TiO. *Phys. Rev. B* **12**, 4917–4928 (1975).

35. Chen, X. J. et al. Pressure-induced phonon frequency shifts in transition-metal nitrides. *Phys. Rev. B* **70**, 014501 (2004).

36. Chen, X. J., Zhang, H. & Habermeier, H.-U. Effects of pressure on the superconducting properties of magnesium diboride. *Phys. Rev. B* **65**, 144514 (2002).

37. Liua, H. Y., Naumova, I. I., Hoffmannb, R., Ashcroftc, N. W. & Hemleyd, R. J. Potential high-T_c superconducting lanthanum and yttrium hydrides at high pressure. *Proc. Natl Acad. Sci. USA* **114**, 6990–6995 (2017).

38. Hopfield, J. J. On the systematics of high T_c in transition metal materials. *Physica* **55**, 41–49 (1971).

39. Eiling, A. & Schilling, J. S. Pressure and temperature dependence of electrical resistivity of Pb and Sn from 1-300 K and 0-10 GPa use as continuous resistive pressure monitor accurate over wide temperature range; superconductivity under pressure in Pb, Sn and In. *J. Phys. F. Met. Phys.* **11**, 623–639 (1981).

40. Zha, X.-H. et al. Intrinsic structural, electrical, thermal, and mechanical properties of the promising conductor Mo$_2$C MXene. *J. Phys. Chem. C.* **120**, 15082 (2016).

41. Liu, Y. Z., Jiang, Y. H., Zhou, R., Liu, X. F. & Feng, J. Elastic and thermodynamic properties of Mo$_2$C polymorphs from first principles calculations. *Ceram. Int.* **41**, 5239–5246 (2015).

42. Woollam, J. A. & Chu, C. W. High-pressure and low-temperature physics (Springer Science & Business Media, 2012).

43. Suderow, H., Tissen, V. G., Brison, J. P., Martínez, J. L. & Vieira, S. Pressure induced effects on the fermi surface of superconducting 2H-NbSe$_2$. *Phys. Rev. Lett.* **95**, 117006 (2005).

44. Qi, Y. et al. Superconductivity in Weyl semimetal candidate MoTe$_2$. *Nat. Commun.* **7**, 11038 (2016).

45. Pan, X. C. et al. Pressure-driven dome-shaped superconductivity and electronic structural evolution in tungsten ditelluride. *Nat. Commun.* **6**, 7805 (2015).

46. Tinkham, M. Introduction to superconductivity (McGraw-Hill, 1996).

47. Spivak, B., Zyuzin, A. & Hruska, M. Quantum superconductor-metal transition. *Phys. Rev. B* **64**, 132502 (2001).

48. Song, J. C., Reizer, M. Y. & Levitov, L. S. Disorder-assisted electron-phonon scattering and cooling pathways in graphene. *Phys. Rev. Lett.* **109**, 106602 (2012).

49. Wang, H. et al. High-quality monolayer superconductor NbSe$_2$ grown by chemical vapour deposition. *Nat. Commun.* **8**, 394 (2017).

50. Navarro-Moratalla, E. et al. Enhanced superconductivity in atomically thin TaS$_2$. *Nat. Commun.* **7**, 11043 (2016).

51. Özer, M. M., Jia, Y., Zhang, Z., Thompson, J. R. & Weitering, H. H. Tuning the quantum stability and superconductivity of ultrathin metal alloys. *Science* **316**, 1594–1597 (2007).

52. Crauste, O., Couëdo, F., Bergé, L., Marrache-Kikuchi, C. & Dumoulin, L. Destruction of superconductivity in disordered materials: a dimensional crossover. *Phys. Rev. B* **90**, 060203 (2014).

53. Simonin, J. Surface term in the superconductive Ginzburg-Landau free energy: Application to thin films. *Phys. Rev. B* **33**, 7830–7832 (1986).

54. Zhang, C. et al. Quantum griffiths singularities in TiO superconducting thin films with insulating normal states. *NPG Asia Mater.* **11**, 76 (2019).

55. Gurvitch, M. et al. Effects of disorder on the transition temperature and transport properties of a low-T_c A15 superconductor: Mo$_3$Ge. *Phys. Rev. Lett.* **41**, 1616–1619 (1978).

56. Chen, X. H. et al. Correlation between the residual resistance ratio and magnetoresistance in MgB$_2$. *Phys. Rev. B* **65**, 024502 (2001).